JMEPEG (2012) 21:1919–1923
DOI: 10.1007/s11665-011-0106-y
©ASM International
1059-9495/$19.00

Flow Behavior and Mechanical Properties of a High Silicon Steel Associated with Dynamic Strain Aging

J.M. Akhgar and S. Serajzadeh

(Submitted March 27, 2011; in revised form November 24, 2011)

Flow behavior of two grades of steel including a high silicon (HS) steel and a plain low carbon steel as the reference were considered in this work. Tensile testing at temperatures varying between 25 and 550 °C and different strain rates in the range of 4×10^{-5} to 0.1 s^{-1} were conducted and the mechanical properties, such as elongation at fracture point and strain rate sensitivity were then determined. It is observed that for both steels, dynamic strain aging occurs in the employed deformation conditions, however, the region of serrated flow and the type of the serration were somehow different. For the case of the HS steel, the serrated flow region is shifted to the higher temperatures and also, the activation energy for appearance of dynamic strain aging increases as well.

Keywords dynamic strain aging, high silicon steel, tensile test

1. Introduction

Dynamic strain aging occurs in dilute alloy systems mainly at cold or warm temperatures and consequently it changes the flow behavior of deforming material. Flow stress and the rate of work hardening increases while the elongation to fracture point and strain sensitivity decreases significantly. Accordingly, prediction of dynamic strain aging in engineering materials especially those deformed at cold and warm deformation regions is important to accurately determine the required energy for metal processing as well as to assess the workability of deforming metal (Ref 1). In this regard, several works have been performed to study dynamic strain aging and serrated flow in metals and alloys including different grades of steels. For instance, Li and Leslie (Ref 2) have studied dynamic strain aging and its influence on the subsequent mechanical properties of different grades of carbon steels. Sachdev (Ref 3) has studied dynamic strain aging by means of tensile testing at various temperatures in various steel grades including low carbon, dual phase, and interstitial free steels. Taheri et al. (Ref 4) have studied the effects of carbon and nitrogen on the occurrence of dynamic strain aging in low carbon (LC) steels. They showed that nitrogen content is a significant factor responsible for occurrence of dynamic strain aging particularly at low temperatures due to its higher mobility and concentration. Kim and Kim (Ref 5) have utilized tensile test to study dynamic strain aging in piping steels. They observed that effect of dynamic strain aging is decreased compared to similar grade carbon steel which they attributed this phenomenon to the effect of high manganese content within the employed steel. Flow behavior of martensitic stainless steel has been studied by Gupta et al. (Ref 6). They performed tensile testing at various strain rates 2×10^{-5} to 10^{-2} s^{-1} and temperatures 25-500 °C. They found that the dominant types of serrated flow are mainly of types A and B. Wagner et al. (Ref 7) have studied dynamic strain aging in heat affected zone after welding of C-Mn steels. They have imposed the thermal cycles to the steel as it occurs under real welding conditions and then the phenomenon of dynamic strain aging was investigated in heat-treated steel by means of tensile testing. Zeghib and Klepaczko (Ref 8) have investigated flow behavior and work hardening characteristics of mild steel in the range of room temperature to 500 °C and accordingly, they have proposed a model based on dislocation theory to describe plastic deformation behavior of the steel. Xu et al. (Ref 9) have studied the kinetics of dynamic strain aging in a low alloy steel utilizing tensile testing in the range of 25-400 °C and they have distinguished different modes of serrated flow in the steel. The effects of chromium and boron on the flow behavior of low alloy steels have been studied in Ref 10 while in this study, compression testing has been used to investigate dynamic strain aging in warm working region. Molaei and Ekrami (Ref 11) have studied the influence of dynamic strain aging on subsequent mechanical properties of dual phase steels. The effect of dynamic strain aging on mechanical properties and flow behavior of micro-alloyed steels (Ref 12, 13), pearlitic steels (Ref 14, 15), and Hadfield manganese steel (Ref 16) have also been conducted using tensile tests at different temperatures and strain rates.

Regarding the existing literature, it can be found that due to the complex inter-connection among chemical composition, temperature and strain rate more studies on different kinds of steels are still of help to understand flow stress behavior associated with dynamic strain aging phenomenon. In this study, utilizing tensile test at temperatures ranging room temperature to 550 °C, and strain rates varying between 4×10^{-5} to 10^{-1} s^{-1} the dynamic strain aging phenomenon for two grades of steel including a plain LC steel as the reference material and a high silicon (HS) steel is studied and the occurrence of dynamic strain aging under cold and warm forming conditions and its effects on flow stress behaviors of the steels are determined.

J.M. Akhgar and **S. Serajzadeh**, Department of Materials Science and Engineering, Sharif University of Technology, Azadi Ave., PO Box 11155-9466, Tehran, Iran. Contact e-mails: akhgar@mehr.sharif.edu and serajzadeh@sharif.edu.

2. Experimental Procedures

Two grades of steels including a plain LC steel and a LC HS steel were examined in this work. The chemical compositions of the employed steels are given in Table 1. As-received bars were first heated up to 900 °C for the LC steel and 930 °C for the HS steel for 30 min and then air cooled to remove pervious hot-rolled structures. Then, tensile samples were prepared according to ASTM E08 and also, optical microscopy was performed to determine the initial microstructures of the steels and ferrite mean grain size of LC steel was also calculated using lineal analysis. Tensile tests (on heating) were then conducted to assess the stress-strain behaviors of the steels while these experiments were carried out at the temperatures in the range of 25 to 550 °C and the mean strain rates of 4×10^{-5} to 10^{-1} s^{-1}. Finally, the stress-strain curves were analyzed and the strain rate sensitivity was calculated at different temperatures using the power law constitutive equation.

3. Results and Discussion

Figure 1 shows the microstructures of the steels. It is observed that the microstructure of the LC steel consists of equiaxed ferrite grains with the mean grain size of 31 μm in addition to about 4% volume fraction of pearlite while the initial microstructure of the HS steel shows a dispersed pearlite structure with the volume fraction of about 30% within ferrite matrix. Apparently, the steels had different microstructures and as a result, they have shown different mechanical behaviors. Figure 2 and 3 show the typical stress-strain behaviors of the steels achieved by tensile tests at different strain rates and temperatures. It is seen that both steels show serrated flow under certain deformation conditions as well as the work-hardening exponent increases during serrated yielding as displayed in the figure. For instance, the work-hardening exponent, i.e., the slope of logarithm stress versus logarithm strain diagram, of the HS steel at 300 °C and strain rates of 4×10^{-5} and 6×10^{-3} s^{-1} was calculated as 0.37 and 0.22, respectively, while this parameter for the same deformation conditions was determined as 0.43 and 0.26, respectively, for the LC steel. The higher amount of *n*-value shows extensive work-hardening associated with dynamic strain aging during deformation in strain rate of 4×10^{-5} s^{-1}. However, it should be noted that the temperature and strain rate regions of serrated flow are different, the types of serrations are not the same in these steels, and also the amplitudes of oscillations are smaller in the HS steel compared to the LC one as it is observed in Fig. 2. According to the literature the serration types may be categorized as A-, B-, C-, D-, and E-types (Ref 1). This classification has been done regarding the appearance of serrations on the stress-strain curves. It is observed that for both steels the serrations are mainly of A- and B-types or their combination. However, in the HS steel serrations of type "irregular A" is also can be seen at moderate strain rates in the order of 10^{-4} to 10^{-3} s^{-1}, given to the deformation temperature as displayed Fig. 2(b) and (d) while at higher strain rates, the serrations are vanished totally. As it has been reported (Ref 1), type B serrations occur at low strain rates and small strains owing to repeated locking and unlocking of mobile dislocations leading to discontinuous propagation of the slip bands while type A serrations mostly occur at higher strain rates, i.e., strain rates higher than 10^{-4} s^{-1} for the employed steels, as a result of occurrence and propagation of deformation bands (Ref 1).

Note that the differences in strain aging behaviors of the employed steels may be attributed to the different chemical compositions of the steels as well as their initial microstructures. In pearlite structures, the ferrite layers are too thin to allow dislocation pining and multiplication or in other words, the strain aging effect is expected to be reduced in microstructures containing high volume fraction of pearlite (Ref 17) such as the HS steel examined in this work. Thus, the higher amount of pearlite in the HS steel can lead a weaker effect of dynamic strain aging on flow stress behavior of the steel. Furthermore, silicon and manganese alloys elements can also alter aging behavior of steels through the interaction with the interstitial atoms. For instance, in steels with high manganese content as the HS steel examined in this work, formation of Mn-C and Mn-N pairs can lead to the reduction of mobility of interstitial

Table 1 Chemical composition of the steels employed in this work (wt.%)

Steel	C	Mn	Si	P (Max)	S (Max)	Cr (Max)	N, ppm	B, ppm
HS	0.11	1.3	0.80	0.025	0.025	0.08	110	11
LC	0.07	0.55	0.03	0.03	0.03	0.07	80	6

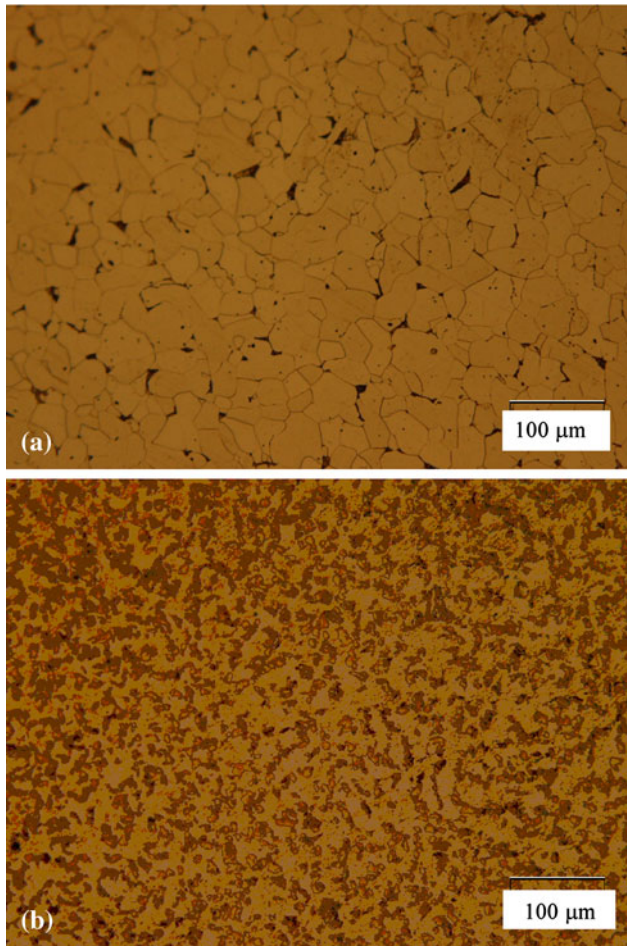

Fig. 1 Initial microstructures of the employed steels: (a) low carbon steel, (b) high silicon steel

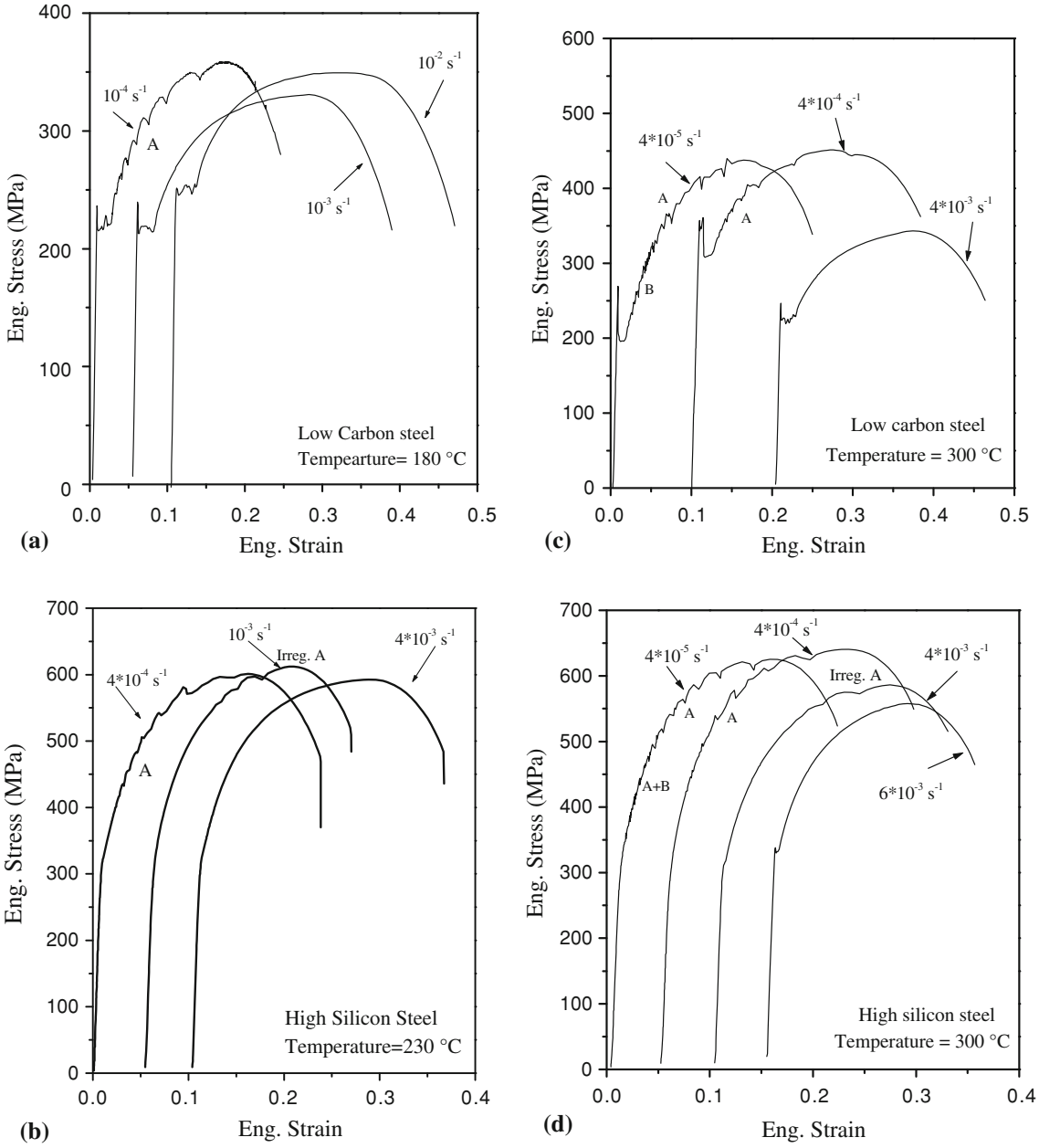

Fig. 2 Stress vs. strain curves achieved at different strain rates: (a) 180 °C, low carbon steel; (b) 230 °C, high silicon steel; (c) 300 °C, low carbon steel; (d) 300 °C, high silicon steel

atoms which in turn this leads to shifting the onset of dynamic strain aging to higher temperatures as well as reducers aging effect (Ref 2). Diagrams of the logarithm of mean strain rate versus the reciprocal of temperature for both steels are shown in Fig. 3. This figure clearly shows the regions of serrated flow and smooth yielding. Regarding this figure, the appearance and/or terminal of serrated flow may be expressed by the Arrhenius-type equation as below

$$\dot{\varepsilon} = A \exp\left(-\frac{Q}{RT}\right) \qquad \text{(Eq 1)}$$

where $\dot{\varepsilon}$ is the applied strain rate, A is a frequency factor, T absolute temperature, R is the gas constant, and Q is the activation energy. For the case of the HS steel, appearance of serrated flow region is shifted to higher temperatures compared to LC steel while the activation energies for appearance of dynamic strain aging were determined as 72.3 and 98.5 (kJ/mol) for the LC and the HS steels, respectively. For the LC steel the appearance activation energy is close to activation energies for diffusion of nitrogen (74 kJ/mol) and carbon (84 kJ/mol) in ferrite indicating that both interstitial elements are responsible for occurring dynamic strain aging. The similar results have been reported in other works (Ref 4, 17). However, for the case of the HS steel, the activation energy increases to 98.5 kJ/mol and the region of serrated flow becomes smaller as compared to that for LC steel. It may be attributed to the effect the stress field and dragging force around substitutional atoms (Ref 1, 2), i.e., silicon and particularly manganese atoms, on mobility of interstitial elements within the ferrite as explained above.

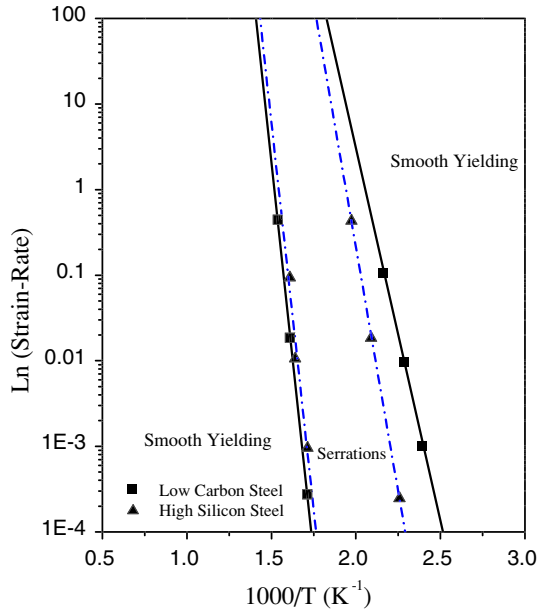

Fig. 3 Serrated flow region as a function of temperature and strain rate

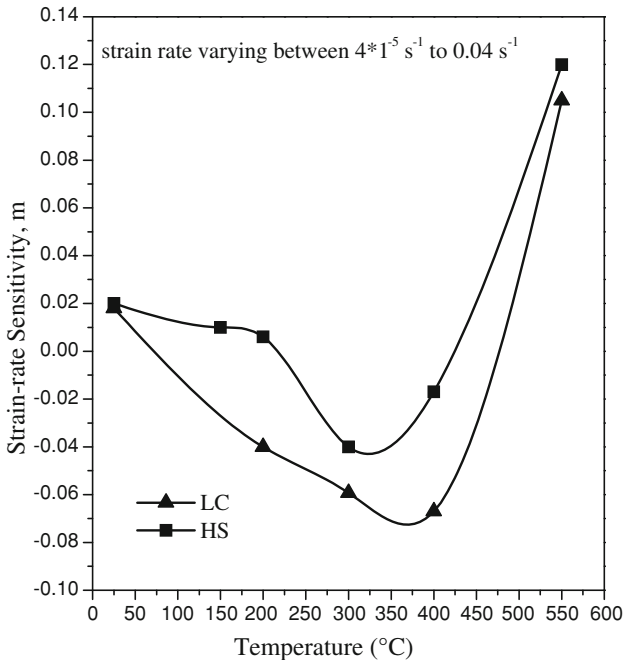

Fig. 4 Variation of strain rate sensitivity with respect to temperature

As a result, it is expected that dynamic strain aging shows a weaker effect on the work-hardening exponent as well as the mechanical properties of the HS steel. Figure 4 shows the strain rate sensitivity for the steels as a function of temperature. As it is expected, negative rate sensitivity is observed in both steels, however, the region for the negative rate sensitivity becomes smaller for the HS steel as well as its intensity is reduced that shows the weaker influence of dynamic strain aging on the mechanical properties in comparison with the LC steel. Figure 5 illustrates the variations of elongation at fracture point for both steels. The variation

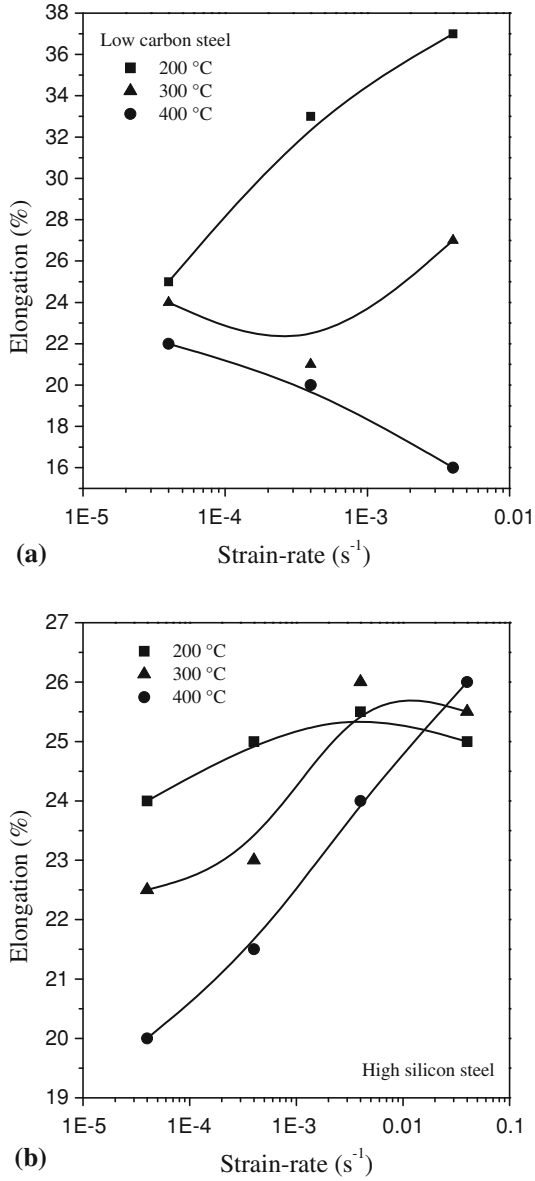

Fig. 5 Variation of elongation with respect to strain rate: (a) the low carbon steel, (b) the high silicon steel

of elongation versus strain rate is consistence with the calculated rate sensitivity parameter. However, the reduction in elongation due to dynamic stain aging is smaller in the HS steel. Furthermore, Fig. 6 shows the variations of tensile strength with respect to temperature for both steels. The maximum increasing in tensile strength of the LC steel is about 35% with respect to the non-aged conditions at room temperature while for the case of the HS steel, it reaches to about 8% again illustrating the weaker effect of dynamic strain aging in the HS steel.

4. Conclusion

In this work, the flow behaviors of two grades of steel were examined employing tensile test at various temperatures and

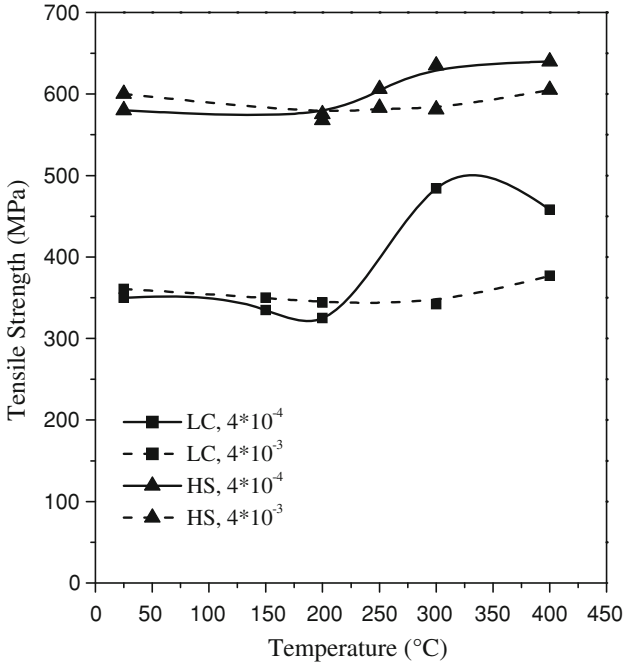

Fig. 6 Variations of tensile strength vs. temperature

strain rates. It is observed that dynamic strain aging occurs in both steels, however, the effect of dynamic strain aging in the HS steel is weaker because of the effects of silicon and manganese on the mobility of interstitial atoms in ferrite as well as higher volume fraction of pearlite. The activation energy for appearance of dynamic strain aging increases to 98.5 kJ/mol in HS steel and on the other hand, the effect of dynamic strain aging on mechanical properties are decreased compared to the LC steel. In addition, appearance of serrations on the stress-strain curves changes from A- and B-types in the LC steel to combination of A-, irregular A-, and B-types in the HS steel.

References

1. J.M. Robinson and M.P. Shaw, Microstructural and Mechanical Influences on Dynamic Strain Aging Phenomena, *Int. Mater. Rev.*, 1994, **39**, p 113–122
2. C.C. Li and W.C. Leslie, Effects of Dynamic Strain Aging on the Subsequent Mechanical Properties of Carbon Steels, *Metall. Trans. A*, 1978, **9**, p 1765–1775
3. A.K. Sachdev, Dynamic Strain Aging of Various Steels, *Metall. Trans. A*, 1982, **13**, p 1793–1797
4. A. Karimi Taheri, T.M. Maccagno, and J.J. Jonas, Dynamic Strain Aging and the Wire Drawing of Low Carbon Steel Rods, *ISIJ Int.*, 1995, **35**, p 1532–1540
5. J.W. Kim and I.S. Kim, Investigation of Dynamic Strain Aging in SA106 Gr.C Piping Steel, *Nucl. Eng. Des.*, 1997, **172**, p 49–59
6. C. Gupta, J.K. Chakravartty, S.L. Wadekar, and J.S. Dubey, Effect of Serrated Flow on Deformation Behavior of AISI, 403 Stainless Steel, *Mater. Sci. Eng. A*, 2000, **292**, p 49–55
7. D. Wagnor, J.C. Moreno, and C. Prioul, Dynamic Strain Aging Sensitivity of Heat Affected Zones in C-Mn Steels, *J. Nucl. Mater.*, 1998, **252**, p 257–265
8. N.E. Zeghib and J.R. Klepaczko, Work Hardening of Mild Steel Within Dynamic Strain Aging Temperature, *J. Mater. Sci.*, 1996, **31**, p 6085–6088
9. S. Xu, X.Q. Wu, E.H. Han, and W. Ke, Effects of Dynamic Strain Aging on Mechanical Properties of SA508 Class 3 Reactor Pressure Vessel Steel, *J. Mater. Sci.*, 2009, **44**, p 2882–2889
10. A.O. Humpherys, S.D. Liu, M.R. Toroghinezad, and J.J. Jonas, Effect of Chromium and Boron Additions on the Warm Rolling Behavior of Low Carbon Steels, *ISIJ Int.*, 2002, **42**, p S52–S56
11. M.J. Molaei and A. Ekrami, The Effect of Dynamic Strain Aging on Subsequent Mechanical Properties of Dual-Phase Steels, *J. Mater. Eng. Perform.*, 2010, **19**, p 607–610
12. S. Gunduz, Dynamic Stain Aging Effects in Niobium Micro-Alloyed Steel, *Ironmaking Steelmaking*, 2002, **29**, p 341–346
13. S. Gunduz and R.C. Cochrane, Effects of Dynamic Strain Aging on Mechanical Properties of Vanadium Microalloyed Steel, *Mater. Sci. Technol.*, 2003, **16**, p 422–428
14. B.M. Gonzalez, L.A. Marchi, E.J. Fonseca, P.J. Modenesi, and V.T.L. Buono, Measurement of dynamic strain aging in pearlitic steels by tensile test, *ISIJ Int.*, 2003, **43**, p 428–432
15. A.R. Kohandehghan, A.R. Sadeghi, J.M. Akhgar, and S. Serajzadeh, Investigation into Dynamic Strain Aging Behaviour in High Carbon Steel, *Ironmaking Steelmaking*, 2010, **37**, p 155–160
16. Y.N. Dastur and W.C. Leslie, Mechanism of Work Hardening in Hadfield Manganese Steel, *Metall. Trans. A*, 1980, **10**, p 749–759
17. E.O. Hall, *Yield Point Phenomena in Metals and Alloys*, Plenum Press, New York, 1970